

The antifungal activity and mechanism of Perillaldehyde and its stabilized encapsulation technology for fruit preservation



Chen Kang ^{a,1}, He Zhang ^{a,1}, Cui Sun ^{a,b}, Jinping Cao ^a, Han Yang ^a, Jiebiao Chen ^a, Yue Wang ^a, Chongde Sun ^{a,b,*}

^a Laboratory of Fruit Quality Biology / The State Agriculture Ministry Laboratory of Horticultural Plant Growth, Development and Quality Improvement / Horticultural Products Cold Chain Logistics Technology and Equipment National-Local Joint Engineering Laboratory / Zhejiang Provincial Key Laboratory of Integrative Biology of Horticultural Plants, Zhejiang University, Hangzhou 310058, PR China

^b Hainan Institute of Zhejiang University, Sanya 572000, PR China

ARTICLE INFO

Keywords:

Perillaldehyde
Antifungal activity
2-hydroxypropyl- β -cyclodextrin
Encapsulation technology
Fruit preservation

ABSTRACT

Perillaldehyde (PAE), an essential oil extracted from perilla (*Perilla frutescens* (L.) Britt.), exhibits excellent antioxidant and antimicrobial activity. In this study, we found that the antifungal mechanism of PAE was attributed to the stimulation of ROS levels, destruction of mitochondrial function, and induction of spore apoptosis. Transcriptomic analysis showed that the gene expression pattern of *Botrytis cinerea* significantly changed after PAE treatment, and the differentially expressed genes (DEGs) were mainly involved in the MAPK signaling pathway and cell wall integrity pathway. For the better utilization of PAE for fruit preservation, the inclusion complex (IC) of PAE and hydroxypropyl- β -cyclodextrin was successfully synthesized by ultrasonic-assisted method, as proved by UV-vis spectroscopy, fourier transform infrared spectroscopy, thermal properties analysis, scanning electron microscopy, and ¹H NMR. It was demonstrated that water solubility and thermal stability of PAE/HP/CD-IC were significantly improved compared to pure PAE. Furthermore, both *in vitro* and *in vivo* antifungal assessment showed that PAE/HP/CD-IC was effective for inhibiting *B. cinerea*. Overall, our results indicated that PAE/HP/CD-IC had promising antifungal activity, water solubility and thermal stability, which provided a theoretical basis for the utilization of PAE/HP/CD-IC for fruit preservation.

1. Introduction

Pathogenic fungi cause severe deterioration of fresh fruit and vegetables, leading to substantial losses to the food industry (Liu et al., 2020). Among them, *Botrytis cinerea*, a pathogenic fungus that is ubiquitous in fruit and vegetables, causing devastating diseases and huge economic loss annually (He et al., 2019). Besides, pathogenic fungus *Alternaria alternata*, *Penicillium expansum* and *Penicillium italicum* also have wide host range on fresh fruit. Recently, the management of fungal infection relies heavily on chemical agents owing to the low cost and convenient utilization. Nevertheless, excessive use of them often causes undesirable problems, such as development of resistance and chemical toxicity, posing tremendous challenges on environment and human health (Romanazzia et al., 2016). Therefore, developing green botanical fungicides as attractive alternatives to chemical fungicides is of great importance.

Numerous studies have reported that essential oils are promising natural volatile compounds for food preservation. Perillaldehyde (PAE), an essential oil originated from perilla (*Perilla frutescens* (L.) Britt.), has been extensively used as flavor ingredient and food additive in recent years (Tian et al., 2019). It also shows excellent antimicrobial activity with little or no adverse effects, as implicated by a volatility test using the air washer (Sato et al., 2006). However, previous studies about the antifungal activity of PAE mainly focused on food-source fungi such as *Aspergillus niger*, *Aspergillus flavus* and *Ceratocystis fimbriata* (Tian et al., 2015; Pan et al., 2020; Zhang et al., 2018). To the best of our knowledge, there are few reports on PAE about the inhibitory effect and mechanism of common postharvest fungal pathogens.

Most of the essential oils are water-insoluble and sensitive to heat owing to their physical and chemical properties, causing restrictions for further utilization. In recent years, molecular encapsulation by the delivery system has been reported to be a practical method to enhance the

* Correspondence to: Zhejiang University, Zijingang Campus, Hangzhou 310058, PR China.

E-mail address: adesun2006@zju.edu.cn (C. Sun).

¹ These authors contributed equally to this work.

water solubility and thermal stability of hydrophobic molecules (Astray et al., 2009). 2-Hydroxylpropyl- β -cyclodextrin (HP β CD), a hydroxyalkyl derivative, is a promising alternative to α -, β - and γ -CDs, with improved water solubility and biological properties (Gao et al., 2023). Owing to its advantages, HP β CD has been extensively applied in the food and medicine industry. According to Yildiz et al. (2019), the cinnamaldehyde/CD-IC NFs showed higher temperature stability and enhanced water solubility, which was potentially applicable in food, oral-care, healthcare, and pharmaceuticals. Jiang et al. (2021) reported that the antifungal properties of tea tree oil towards *Monilinia fructicola* were more stable and long-lasting after being incorporated with HP β CD. Furthermore, Gao et al. (2022b) demonstrated that the fabrication HP β CD/PMT-IC-NF had better solubility, thermostability and antifungal activities compared to Pyrimethanil (PMT), which provided new insights in the application of new pesticide preparations. Our research team also found that the encompassment of thymol and carvacrol with HP β CD improved the water solubility, thermal stability and antifungal capacity compared to the monomeric molecules (Sun et al., 2021, 2022). Thus, encapsulation by HP β CD to form the inclusion complex was proved to be an effective strategy for the application of essential oils.

In this study, the inhibitory effects of PAE towards common post-harvest fungal pathogens were evaluated on the PDA plate, and the antifungal mechanisms were investigated combining microscopic observation and transcriptome analysis. In order to stabilize PAE for fruit preservation, HP β CD was used as wall materials to encapsulate PAE and the resulting inclusion complex was characterized by a series of techniques. In addition, the antifungal capacity of PAE/HP β CD-IC was evaluated both *in vitro* and *in vivo*. The current study aimed to provide a theoretical basis for the utilization of PAE and develop a stabilized inclusion complex for fruit preservation.

2. Materials and methods

2.1. Materials

The fruit pathogen of *B. cinerea* was isolated from decayed tomato fruit, with the strain number of B05.10. Tomato (*Solanum lycopersicum* L.) and strawberry (*Fragaria × ananassa* Duch.) fruit used in this study were harvested at the ripening stage from a local farm in Hangzhou city, China. After transported to laboratory, these fruit were surface sterilized with 0.2% (v/v) sodium hypochlorite solution (NaClO) for further assay. All the reagents and solvents used in this article were of analytical grade.

2.2. Microscopic observation of *B. cinerea* after PAE treatment

2.2.1. Sample preparation

The fungal suspension of *B. cinerea* was obtained by 10 mL of PDB liquid medium after scraping from the cultures. Then, the PAE solution was added to the fungal suspension with the final concentration of 0, 0.5 and 1 μ L/mL, respectively. After constant shaker incubation at 26 °C/200 rpm for 6 h, the suspension was filtered with sterile gauze to remove mycelia.

2.2.2. Scanning electron microscopy (SEM) and transmission electron microscopy (TEM)

The SEM and TEM observation was performed as previously described (Liu et al., 2022), using Hitachi SU-8010 (Hitachi, Japan) and Hitachi H-7650 (Hitachi, Japan), respectively. The spores used for SEM and TEM were collected and fixed as described in Method S1.

2.2.3. Determination of spores apoptosis and necrocytosis

Propidium Iodide (PI) staining and Hoechst 33342 staining were applied for the detection of apoptotic and necrotic spores, with a concentration of 20 μ g/mL. After dying for 20 min at room temperature, the samples were observed using a confocal laser scanning microscope LSM780 (ZEISS, Germany), with excitation at 535/346 nm and emission

at 615/460 nm, respectively.

2.2.4. Measurement of intracellular ROS content

Intracellular ROS content was detected using the Reactive Oxygen Species Assay Kit (Yeasen, China) according to the manufacturers' instruction. The concentration of DCFH-DA was adjusted to 10 μ mol/L before staining, and the excitation and emission wavelength were set as 488 nm and 525 nm, respectively.

2.2.5. Analysis of mitochondrial membrane potential

Detection of mitochondrial membrane potential (MMP) of *B. cinerea* was performed using Mito-Tracker Red CMXRos (Solarbio, China). The concentration of Mito-Tracker was adjusted to 1 μ mol/L before staining, and the excitation and emission wavelength were set as 579 nm and 599 nm, respectively.

2.3. Transcriptome analysis of *B. cinerea* after PAE treatment

Total RNA was extracted using Fungal RNA Extraction Kit (Omega, USA), with three biological replicates for each treatment. The library construction and RNA sequencing were performed by BGI (Wuhan, China). The constructed libraries were sequenced by the Illumina HiSeq 4000 sequencing platform to obtain clean raw read. After filtered with SOAPnuke (Version 1.5.2), all clean reads were mapped to the reference genome [Ensembl Genomes GCA_000143535.4_Botrytis_cinerea_B05.10]. The expression levels of genes were estimated by the values of fragments per kilobase of transcript per million mapped reads (FPKM). Kyoto Encyclopedia of Genes and Genomes (KEGG) pathway enrichment analysis of annotated differentially expressed genes was performed by clusterProfiler R software as described by Kang et al. (2022).

2.4. Synthesis of PAE/HP β CD-IC using the ultrasonic-assisted method

Ultrasonic-assisted method was adopted to prepare the PAE/HP β CD inclusion complex according to Sun et al. (2022). Firstly, 67.82 g of HP β CD was homogenized in 200 mL of 20% ethanol phosphate buffer solution (pH = 6.8), followed by adding 13.22 mL of PAE-ethanol solution (containing 6.61 g of PAE) under the condition of magnetic stirring. Then, ultrasonic treatment (65 w, 25 °C) was performed for 30 min in order to form the inclusion complex. Finally, the mixed solution was lyophilized for 3 d and ground into fine powder for further experiment.

2.5. Characterization and measurements of PAE/HP β CD-IC

2.5.1. Ultraviolet-visible absorption and fluorescence spectroscopy

The UV-vis and fluorescence spectra were obtained by an UV-2600 spectrophotometer (SHIMADZU, Japan) and fluorescence spectrophotometer (Cary Eclipse, USA), respectively. The stoichiometric ratio for the PAE/HP β CD-IC was also obtained using the maximum fluorescence intensity to the modified Benesi-Hildebrand (B-H) Eqs. (1) and (2) as described by Negi and Singh (2013).

$$1/(F - F_0) = 1/(F' - F_0) + 1/K_a(F' - F_0)[HP\beta CD] \quad (1)$$

$$1/(F - F_0) = 1/(F' - F_0) + 1/K_a(F' - F_0)[HP\beta CD]^2 \quad (2)$$

F_0 and F is the emission intensities in the absence and presence of HP β CD respectively, and F' represents the emission intensity of PAE with the highest HP β CD concentration. K_a represents the association constant.

2.5.2. Fourier transform infrared (FT-IR) spectroscopy

The samples used for FT-IR detection were prepared according to the method of Sun et al. (2021). The FT-IR spectra were obtained by a Fourier transform infrared spectrometer (Thermo Nicolet, USA), with

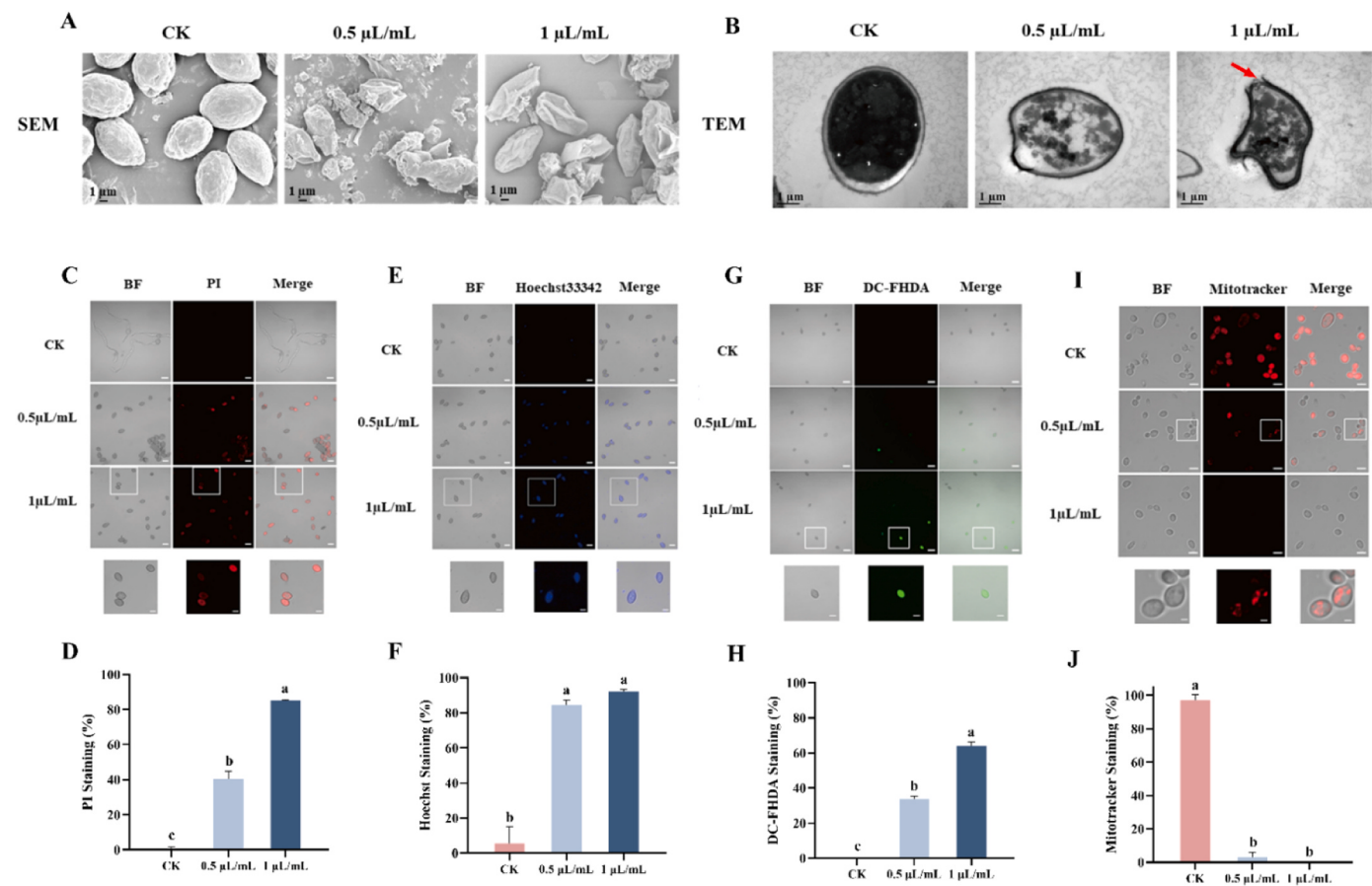


Fig. 1. The morphological and metabolic changes of *B. cinerea* after PAE treatment. (A) Scanning electron microscopy of *B. cinerea*. (B) Transmission electron microscopy of *B. cinerea*. (C and D) PI staining of *B. cinerea*. (E and F) Hoechst33342 staining of *B. cinerea*. (G and H) DC-FHDA staining of *B. cinerea*. (I and J) Mito-Tracker staining of *B. cinerea*. CK, sterilized water treatment. Data were represented as mean \pm standard deviation of six replicates ($n = 6$). Different lowercase letters in the column of the same component represented a significant difference between different groups at $p < 0.05$ level by Tukey testing.

the scanning wavelength range of 400–4000 cm^{-1} .

2.5.3. Proton nuclear magnetic resonance (^1H NMR) spectroscopy

^1H NMR spectra of samples were obtained by 600 NMR spectrometer (Agilent Technology, USA) at room temperature. Briefly, approximately 10 mg of each sample was dissolved in 0.5 mL of deuterated dimethyl sulfoxide ($\text{DMSO}-d_6$) before analysis. The chemical shifts were calibrated by tetramethyl silane (TMS), which were expressed as δ ppm.

2.5.4. Phase solubility analysis

Phase solubility analysis of PAE/HP β CD was performed according to (Zhou et al., 2013) with slight modifications (Method S2). The stability constant K_s (L mol^{-1}) and thermodynamic parameters ΔG were calculated according to the formulas (3) and (4).

$$K_s = \frac{\text{slope}}{S_0 (1 - \text{slope})} \quad (3)$$

$$\Delta G = -RT \ln K_s \quad (4)$$

S_0 represents the solubility of PAE in an aqueous solution without HP β CD. T is the incubation temperature (310 K) and R is the universal gas constant (8.314 J/mol K).

2.5.5. Thermal properties and stability analysis

The thermal properties were evaluated by Thermogravimetric Analysis (TGA) using a thermogravimetric analyzer (NETZSCH Instruments, German), and Differential Scanning Calorimetry (DSC) using differential scanning calorimetry (NETZSCH Instruments, German). The

samples were scanned at a heating rate of $10^\circ\text{C min}^{-1}$, which ranged from 25 to 500°C . The stability of PAE monomer and PAE/HP β CD-IC were analyzed by UV irradiation as described in Method S3.

2.6. In vitro and in vivo antifungal activity of PAE/HP β CD-IC

The *in vitro* antifungal activity of PAE/HP β CD-IC was evaluated on the PDA plate, and the *in vivo* antifungal activity of PAE/HP β CD-IC was conducted on tomato and strawberry fruit, which was described in Method S4.

2.7. Statistical analysis

Data were statistically analyzed using SPSS (Version 20.0, USA) and represented as mean \pm standard deviation (SD) in the figures. Comparisons among groups were carried out using the Tukey multiple range test at $p < 0.05$ level. Figures were drawn using GraphPad Prism (Version 8.0.2, USA).

3. Results and discussion

3.1. The morphological and metabolic changes of *B. cinerea* after PAE treatment

3.1.1. Microscopic observation of spore morphology

In a pilot study, we found that Perillaldehyde (PAE) had promising inhibitory efficiency on fungal pathogens among 11 essential oils (Fig. S1, S2 & S3). As one of the most common and harmful postharvest

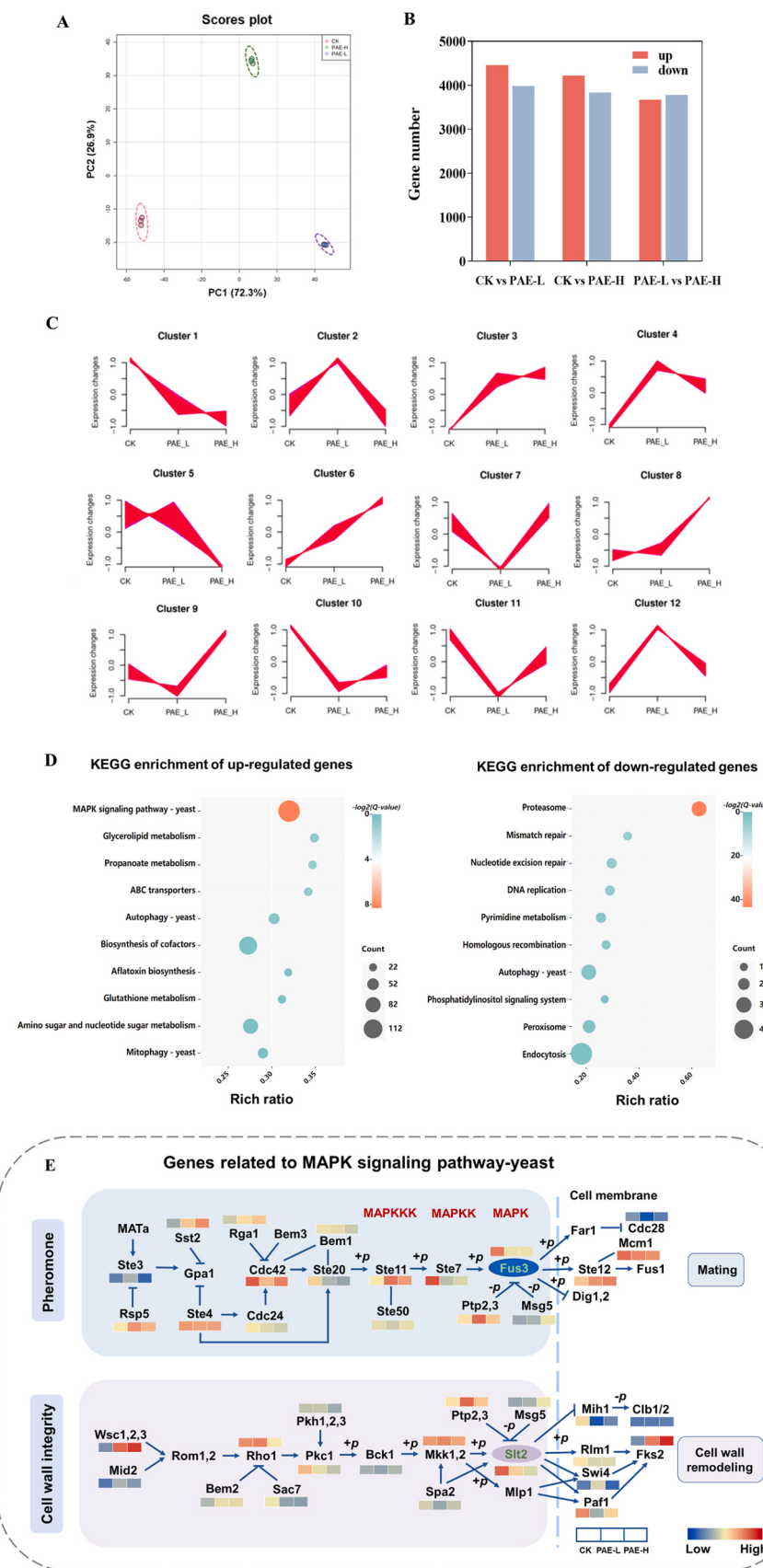


Fig. 2. Transcriptome analysis of *B. cinerea* after PAE treatment. (A) PCA analysis of gene expression. (B) The number of differentially expressed genes. (C) Mfuzz clustering analysis of differentially expressed genes. (D) KEGG enrichment analysis of clustered genes. (E) The expression level of genes related to Yeast-MAPK signaling pathway. Arrows and T symbols represent activation and inhibitory effects, respectively. The color scale represented the gene expression level based on PPKM value. CK, sterilized water treatment. PAE-L, low concentration of PAE treatment (0.5 mg/mL). PAE-H, high concentration of PAE treatment (1 mg/mL).

fungal pathogens, *B. cinerea* was claimed to be a model pathogen in plant disease research (Abbey et al., 2019). Thus, it was selected for further investigation of the antifungal mechanisms of PAE. The concentrations of 0.5 and 1 $\mu\text{L}/\text{mL}$ were chosen for investigation due to the significant suppression on the growth of *B. cinerea* as tested before. As shown by SEM, the spores of the water-treated *B. cinerea* had intact cellular morphology and microscopic structure, with a regular ellipsoid shape. On the contrary, after PAE treatment, the spores appeared shrunken and aggressively crumpled, with the spore structure destroyed and morphology changed greatly (Fig. 1A). Furthermore, TEM showed that the cell wall structure of the control group was uniformly intact and inner structure was dense. However, the ultrastructure of the spores was damaged when posed to 0.5 $\mu\text{L}/\text{mL}$ of PAE treatment, causing the leakage of intracellular components (Fig. 1B). As the PAE concentration increased to 1 $\mu\text{L}/\text{mL}$, the spore cell wall was severely disrupted (marked by the red arrow), accompanied by the loss of cell membrane integrity. The SEM and TEM observation indicated that PAE treatment disrupted the integrity of the cell membrane, leading to spore necrosis and cytoplasmic exocytosis.

3.1.2. Effect of PAE treatment on spore necrocytosis and apoptosis

The integral cell membrane plays an vital role in maintaining the intracellular balance of fungus and in adaptation to environmental conditions. Propidium iodide (PI) was employed to evaluate the integrity of spore membranes. As shown in Fig. 1C and D, no PI staining signal was detected in the control group. However, 40.53% of the spores were stained by PI after treated by 0.5 $\mu\text{L}/\text{mL}$ of PAE, and the staining rate raised by 85.19% when the concentration increased to 1 $\mu\text{L}/\text{mL}$, indicating that PAE treatment caused severe damage to the cell membrane and necrocytosis of *B. cinerea* spores. Apoptosis is a typical programmed cell death pathway, with a symbol of disruption of mitochondrial function (Tang et al., 2022), which can be detected by Hoechst33342. The result showed that the Hoechst33342 staining rate reached to 84.44% and 92.09% after 0.5 and 1 $\mu\text{L}/\text{mL}$ of PAE treatment, which suggested that even low concentration of PAE could induce spore necrocytosis of *B. cinerea* (Fig. 1E and F). The plasma membrane is an important target for antifungals, and the destruction of which could accelerate the necrosis of fungal spores (Shu et al., 2019). Tian et al. (2015) revealed that the membrane integrity of *A. niger* spores has completely lost after 2 $\mu\text{L}/\text{mL}$ of PAE treatment, which was consistent with our current results. It was found that both necrocytosis and apoptosis initiated when fungal spores exposed to PAE treatment. As reported by Yang et al. (2022), intrinsic apoptosis and necroptosis pathways may co-exist to induce cell death of *P. expansum* after bifonazole treatment. Similar results also obtained by Ma et al. (2023) through the treatment of antimicrobial peptide AMP-17 on *Candida albicans*. Liu et al. (2022) also demonstrated that the fluorescence intensity of PI and Hoechst33342 both increased after cold atmospheric plasma (CAP) treatment, indicating that the two cell death pathways may not contradict each other. However, it also has been controversial whether the two processes occur independently or dependently in fungal spores and still remain further explored.

3.1.3. Effect of PAE treatment on intracellular ROS content

Intracellular ROS content is a direct indicator reflecting the level of oxidative stress, which can be detected by 2',7'-dichlorofluorescein diacetate (DCFDA). It can be seen from Fig. 1G that the number of spores with DCFDA signals increased significantly after PAE treatment ($p < 0.05$), whereas no fluorescent signal was observed for spores in the control group. This result suggested that PAE treatment led to the accumulation of intracellular ROS in *B. cinerea*, which coincided with the previous study on *Ceratocystis fimbriata* (Tian et al., 2019). ROS was shown to be both necessary and sufficient for inducing apoptosis in yeast, the production of which might be one of the triggers for spore apoptosis (Hwang et al., 2012).

3.1.4. Effect of PAE treatment on mitochondrial membrane potential

Mitochondrial membrane potential is an essential indicator of mitochondrial function and state. As shown in Fig. 1I, approximately 97.20% of the spores in the control group were labeled with Mito-tracker red, reflecting normal mitochondrial membrane potential. However, the staining rate of Mito-tracker red dropped to 3.15% after 0.5 $\mu\text{L}/\text{mL}$ of PAE treatment (Fig. 1J). Moreover, no spores showed red fluorescence signals at 1 $\mu\text{L}/\text{mL}$ of PAE treatment, suggesting that PAE treatment abolished the mitochondrial membrane potential and disrupted mitochondrial functions of *B. cinerea*. As one of the hallmarks of apoptosis, the disruption of mitochondrial functions echoed to the higher Hoechst33342 staining rate after PAE treatment. Moreover, Tian et al. (2019) indicated that PAE could induce apoptosis by damaging the MMP of *Ceratocystis fimbriata*, thereby increasing membrane permeability, which was coincident with our results.

3.2. Transcriptome analysis further revealed the molecular mechanisms of PAE treatment

We carried out transcriptome analysis to get more understanding of the antifungal mechanism of PAE. The transcriptome analysis generated 57.33 Gb of clean data for three treatments, with three biological replicates in each treatment (Table S). Moreover, clean base Q30 and mapped the percentage of each library were greater than 93% and 89%, indicating the high quality of the sequencing data. RT-qPCR verification were conducted for the related genes, and the relative expression levels of them were coincidental with RNA-seq (Table S1; Fig. S4).

3.2.1. Gene expression pattern after PAE treatment

PCA analysis was conducted based on the sequencing data to check the gene expression profile and to evaluate data quality. As presented in Fig. 2A, the same treatment was clustered together, while samples from different groups were clearly separated. Notably, the CK group and PAE-H group were separated both on PC1 loading and PC2 loading. Thus, PCA analysis revealed that the sequencing data exhibited a good group variation, which was suitable for further biological analysis. Furthermore, the highest number of DEGs were found between CK and PAE-L, including 4474 up-regulated genes and 4000 down-regulated genes (Fig. 2B), which indicated that PAE treatment significantly changed the gene expression pattern of *B. cinerea*.

3.2.2. Analysis of genes expression trends by Mfuzz clustering

Mfuzz clustering analysis was carried out to investigate how the DEGs responded to PAE treatment. As shown in Fig. 2C, all 11,736 DEGs were grouped into 12 clusters. Among them, clusters 3, 6, and 8 showed a consistent tendency with the increase of PAE concentrations, which were classified as up-regulated genes for further analysis. On the contrary, clusters 1 and 5 exhibited an opposite trend with PAE concentrations. These genes were grouped into down-regulated gene after PAE treatment. The cluster of up-regulated genes contains 2940 genes, while the down-regulated cluster contains 1230 genes.

3.2.3. KEGG enrichment analysis of clustered genes

As shown in Fig. 2D, KEGG enrichment analysis was carried out to find out the pivotal pathways correlated with antifungal activity of PAE against *B. cinerea*. We found that the proteasome and mismatch repair were mostly aggregated in the down-regulated genes cluster. Among all the annotated pathways in up-regulated genes cluster, the MAPK signaling pathway-yeast was the most enriched pathway, with a Q-value of 0.0031 and rich factor of 0.3198, respectively. A previous study by Pan et al. (2020) indicated that MAPK signaling pathway played an important role in antioxidant response to PAE treatment, which served as an effector in inducing oxidant damage and cell cycle arrest. These results implied that the alteration of gene expression in MAPK signaling pathway might be related to the inhibitory effect of PAE on *B. cinerea*.

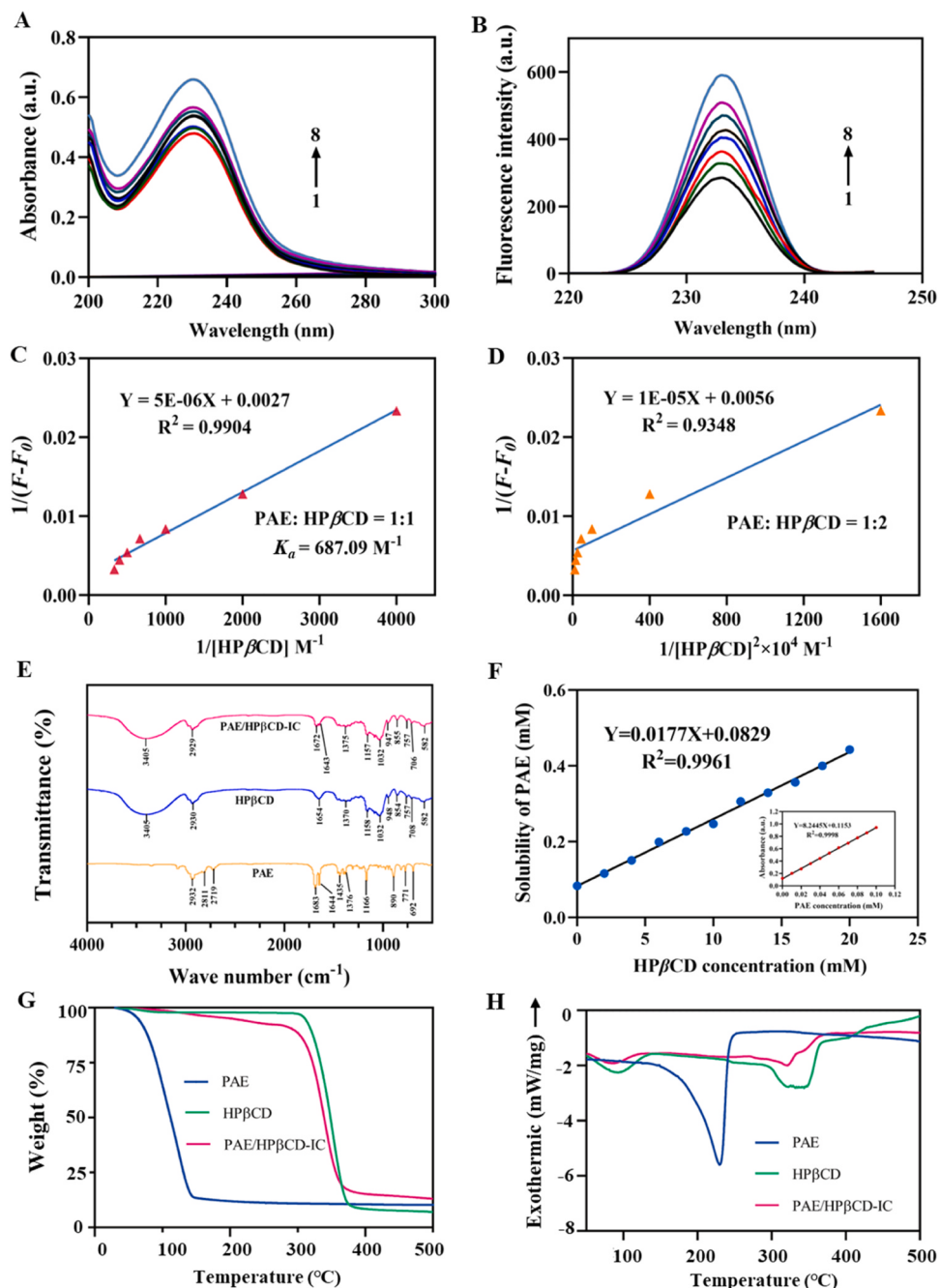


Fig. 3. Preparation and characterization of PAE/HP β CD-IC. (A) The UV-vis absorption spectroscopy of PAE containing different concentrations of HP β CD. The concentrations of HP β CD from 1 to 8 were 0, 1, 2, 4, 6, 8, 10 and 12 mmol/L, respectively. (B) The fluorescence emission spectroscopy of PAE. The concentrations of HP β CD from 1 to 8 were 0, 0.25, 0.5, 1, 1.5, 2, 2.5 and 3 mmol/L, respectively. (C) B-H double reciprocal plot of $1/(F - F_0)$ versus $1/[HP\beta CD]$ for the formation of 1:1 complex. (D) B-H double reciprocal plot of $1/(F - F_0)$ versus $1/[HP\beta CD]^2$ for the formation of 1:2 complex. (E) The Fourier transform infrared spectrometer of PAE, HP β CD and PAE/HP β CD. (F) The phase solubility of PAE/HP β CD-IC. (G) TGA of PAE, HP β CD and PAE/HP β CD. (H) DSC of PAE, HP β CD and PAE/HP β CD.

3.2.4. Gene expression analysis related to MAPK signaling pathway-yeast

As one of the topmost enriched KEGG pathways as described above, the MAPK signaling pathway-yeast was intimately involved in pheromone and cell wall integrity (CWI) pathways. The expression levels of corresponding genes were shown in Fig. 2E based on the FPKM value. It was found that the expression of gene related to pheromone and CWI pathway were significantly altered, indicating that *B. cinerea* underwent cell wall stress situations after PAE treatment. For example, Rho-type GTPase homologous 1 (Rho1) protein plays a vital role in CWI pathway, which was responsible for the biosynthesis of glucan (Bartual et al., 2021). The expression level of corresponding genes first

up-regulated in 0.5 μ L/mL of PAE treatment, whereas down-regulated after posed to higher concentration of PAE. However, the expression level of *Bcin02g08170* was significantly down-regulated, which encoded the key kinase Slt2 involved in CWI pathways. It might be due to the up-regulation of *Ptp2,3* and *Msg5*, which acted as inhibitory factors for both *Fus3* and *Slt2*. As reported by Islahudin et al. (2013), the MAPKKK of *Slt2* was essential for fungi to resist antifungals and maintain cell wall integrity. Taken together, the transcriptome analysis showed that PAE treatment could activated the MAPK signaling pathway of *B. cinerea*, thereby led to cell wall integrity disruption and cell wall remodeling, which was echoed to the microscopic observation and fluorescent

staining results.

3.3. Preparation and characterization of PAE/HP β CD-IC for fungal inhibition and fruit preservation

PAE have an excellent antifungal ability as mentioned above. However, the monomeric form of PAE is water-insoluble and easy to volatilize, which cannot be directly utilized for postharvest fruit preservation. Previous studies have reported that encapsulation of antifungal molecules (*i.e.*, carvacrol and myricetin) with β -cyclodextrin or its derivatives can eliminate these adverse effects by forming the inclusion complex (Yao et al., 2014; Sun et al., 2022). To improve the stability and solubility of PAE for fruit preservation, the ultrasonic-assisted method and freeze-drying method was adopted for the synthesis of PAE/HP β CD-IC. Furthermore, PAE was successfully encapsulated by HP β CD as proved by the following evidence.

3.3.1. UV-vis absorption and fluorescence emission properties of PAE/HP β CD-IC

The inclusion complex of PAE and HP β CD was firstly evaluated using UV-vis absorption spectroscopy. Here, the UV-vis absorption spectra of PAE with different concentrations of HP β CD were shown in Fig. 3A (in

the wavelength range 200–300 nm). It can be found that PAE exhibited a characteristic absorption peak at 230 nm owing to the presence of a benzene ring in the molecule structure of perillaldehyde. Moreover, the absorbance of the peak gradually increased upon the increment of HP β CD concentration, which might be due to the raise of solubility of PAE in the aqueous solution. To further explore the encapsulation properties of PAE/HP β CD-IC, fluorescence emission spectroscopy was conducted for PAE containing different concentrations of HP β CD. We found that PAE exhibited a signal emission peak around 234 nm with the excitation wavelength at 230 nm (Fig. 3B). Similarly, the fluorescence intensity of the peak enhanced with the steady addition of HP β CD, which was coincidence with the study by Sun et al. (2022). Based on the fluorescence spectra, a good-linear relationship was obtained when $1/(F - F_0)$ was plotted against $1/[HP\beta CD]$ ($R^2 = 0.9904$), indicating that the stoichiometric ratio of PAE/HP β CD-IC was 1:1 (Fig. 3C). However, a poor linear correlation was found between $1/(F - F_0)$ and $1/[HP\beta CD]^2$, which excluded the possibility of 1:2 stoichiometries between the PAE and HP β CD molecules (Fig. 3D). Furthermore, the association constant K_a was calculated to be 687.09 M^{-1} , indicating the strong host-guest interactions between PAE and HP β CD. Thus, the result indicated that the PAE molecule was successfully encapsulated into the cavity of HP β CD and the PAE/HP β CD-IC was stably formed after ultrasound

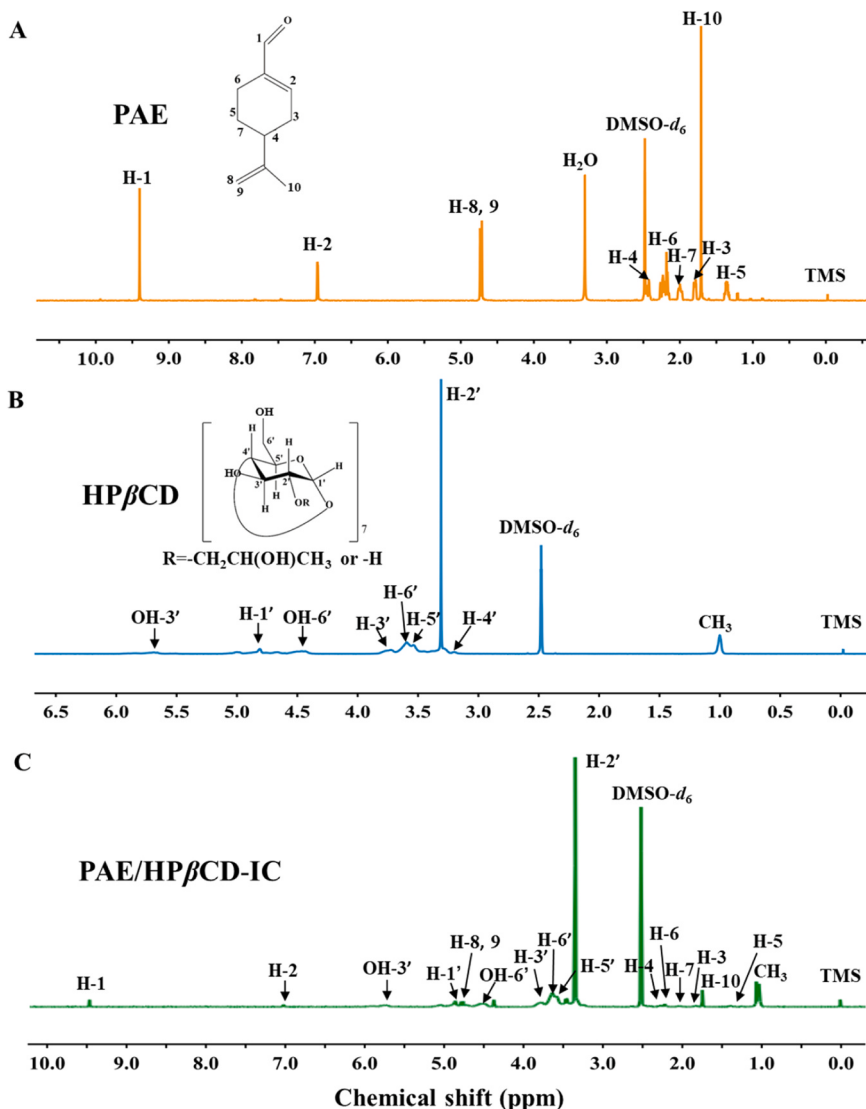


Fig. 4. The proton nuclear magnetic resonance spectroscopy (^1H NMR). (A) PAE, perillaldehyde. (B) HP β CD, 2-hydroxypropyl- β -cyclodextrin. (C) PAE/HP β CD-IC, the inclusion complex of PAE and HP β CD.

treatment.

3.3.2. FT-IR analysis of PAE/HP β CD-IC

FT-IR analysis was another commonly used method to characterize the formation of the inclusion complex. As shown in Fig. 3E, The FT-IR spectrum of PAE presented a medium-intensity absorption peak at 2932 and 2811 cm $^{-1}$, attributing to the C-H bond stretching vibration of methylene and methyl groups. The strong absorption peak at 1683 cm $^{-1}$ was assigned to the stretching vibration peak of aldehyde carbonyl C=O conjugated with -C=C-. Moreover, the peaks at 1644, 1435 and 890 cm $^{-1}$ were due to the stretching vibration of C=C, in-plane bending vibrations of C-H in alkanes and out-of-plane bending vibration of C-H in olefins, respectively (Gao et al., 2022a). The characteristic peaks of HP β CD were observed at 3405 cm $^{-1}$ (for O-H stretching), 2930 cm $^{-1}$ (for C-H stretching), 1645 cm $^{-1}$ (for crystallized water stretching), 1370, 1158 and 1032 cm $^{-1}$ (for C-O stretching) (Cui et al., 2019). However, in the FT-IR spectrum of PAE/HP β CD-IC, the characteristic absorption peaks of PAE at 2811, 1435 and 890 cm $^{-1}$ disappeared and the absorption peak of C=C shifted at 1643 cm $^{-1}$, which may be related to the formation of inclusion complex. These above changes of stretching vibration further confirmed that PAE was successfully incorporated in the hydrophobic cavity of HP β CD.

3.3.3. Phase solubility assay of PAE/HP β CD-IC

The phase solubility analysis of PAE was carried out in aquation solutions at 310 K. As demonstrated in Fig. 3F, the linear equation for PAE solubility in the concentration range of 0–20 mmol/L HP β CD was $Y = 0.0177X + 0.0829$, with a coefficient of 0.9961. The phase solubility diagram obtained was attributed to the A_L-type phase based on the theory of Higuchi and Connors (Higuchi and Connors, 1965). This may be attributed to the formation of a 1:1 inclusion complex between PAE and HP β CD. According to the formulas described above, the stability constant K_S and thermodynamic parameters ΔG was calculated to be 217.36 L mol $^{-1}$ and $-18.71 \text{ kJ mol}^{-1}$, respectively. These results suggested that PAE could be closely bound to HP β CD at 310 K by intermolecular force and that the complexation of PAE with HP β CD was an energy-releasing process. Moreover, the water solubility of PAE was largely improved with the presence of HP β CD, which was further confirmed by the water dissolution study (Fig. 3F). Relevant literature studies also demonstrated that the solubility of perillaldehyde was largely improved by HP β CD, which was another type of cyclodextrin (Gao et al., 2022a). Hence, this result indicated that the stable inclusion complex of PAE and HP β CD was formed and the formation of the complex had an exothermic heat signature.

3.3.4. Thermal properties determination of PAE/HP β CD-IC

The thermal properties of PAE, HP β CD and PAE/HP β CD-IC were further investigated by TGA and DSC measurement. As depicted in Fig. 3G, the PAE sample began to accelerate volatilization around 50 °C and ended volatilization around 150 °C. As for the HP β CD sample, the weight loss was divided into two steps, including evaporation of water below 86.83 °C and high-temperature degradation of HP β CD between 302.16 °C and 387.83 °C. However, PAE/HP β CD-IC thermogram included three weight loss steps: i) evaporation of water below 115 °C, ii) volatilization of PAE below 282 °C and iii) high-temperature degradation of HP β CD around 303 °C. It can be found that the accelerated volatilization temperature of PAE shifted from the original 50–282 °C after being encapsulated with HP β CD, indicating the thermal stability of PAE. It was consistent with a previous report by Yildiz et al. (2019) that the volatilization temperature of cinnamaldehyde moved to 270 °C from the original 170 °C after complexation with HP γ CD.

In addition to TGA, DSC analysis can provide information about the thermodynamic properties of the inclusion complex during combination. Previous studies demonstrated that the weight loss temperature and exothermic peaks of the inclusion complex were generally shifted or disappeared compared with pure host or guest (Tang et al., 2015). The

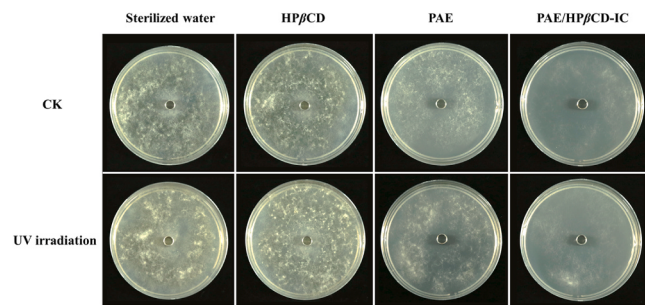


Fig. 5. The stability assessment of PAE/HP β CD-IC after 4 d of inoculation. The concentration of HP β CD and PAE/HP β CD-IC were both 50 mg/mL, and the concentration of PAE monomer was adjusted to the equivalent amount of PAE with PAE/HP β CD-IC. CK represents no UV irradiation treatment.

DSC curve of PAE displayed a broad endothermic peak from 49.5° to 226.2°C, indicating the decomposition process of PAE (Fig. 3H). As for the HP β CD curve, the endothermic peak around 68.8 °C corresponded to the evaporation of water and another endothermic peak at 320.7–348.0 °C was attributed to the high-temperature decomposition. Notably, the endothermic peak of PAE was completely absent in the thermal profile of PAE/HP β CD-IC, which suggested that PAE was successfully incorporated into the cavity of HP β CD and subsequently formed the amorphous complex. Taken together, the above results provided new evidence for the formation of PAE/HP β CD-IC and the enhanced thermal stability of PAE/HP β CD-IC after being incorporated with HP β CD.

3.3.5. ^1H NMR analysis of PAE/HP β CD-IC

The formation of the inclusion complex between host HP β CD and guest PAE were demonstrated and explored by ^1H NMR analysis. It was found that the majority of PAE protons displayed chemical shifts at 1.0–10.0 ppm, which were distinct from the HP β CD protons (3.0–6.5 ppm) (Fig. 4). The hydrogen chemical shifts were changed upon the formation of PAE/HP β CD-IC, and the $\Delta\delta$ (variations of the chemical shifts) values were listed in Table S2 and Table S3. The downward or upward chemical shift changes of protons indicated that the PAE molecules might be entirely entrapped into the cavity of HP β CD (Sun et al., 2021). However, all the $\Delta\delta$ values were ≤ 0.01 ppm, which indicated that no new chemical bonds were generated and the inclusion complex was formed through intermolecular force rather than covalent bonds (Pu et al., 2018). Our findings coincided with previous studies on the formation of myricetin/HP- β -CD (Yao et al., 2014). The above results provided powerful evidence for the successful formation of PAE/HP β CD-IC.

3.3.6. Stability assessment of PAE/HP β CD-IC

UV irradiation treatment is a useful strategy for the stability assessment of essential oils. The inhibitory effects of HP β CD, PAE and PAE/HP β CD-IC on the growth of *B. cinerea* were shown in Fig. 5. After inoculation for 4 d, the colony of *B. cinerea* extended almost to the whole plate in sterilized water and HP β CD treatment. The PAE monomer inhibited the extend of mycelium to some extent, but the antifungal effects tended to decrease after 12 h of irradiance. In contrast, after being incorporated with HP β CD to form the inclusion complex, PAE/HP β CD-IC almost completely inhibited the growth of *B. cinerea*, even under the condition of UV irradiation. This phenomenon may be related to the enhanced stability of PAE after encapsulation by HP β CD, thus retarding the degradation of PAE under UV irradiation. This was consistent with the former study by Wang et al. (2011), who found that FA/HP β CD inclusion complex made FA insensitive to the tested UVB stress. Yuan et al. (2008) also demonstrated that the formation of the inclusion complex of astaxanthin with hydroxypropyl- β -cyclodextrin greatly enhanced the stability of astaxanthin against light and oxygen.

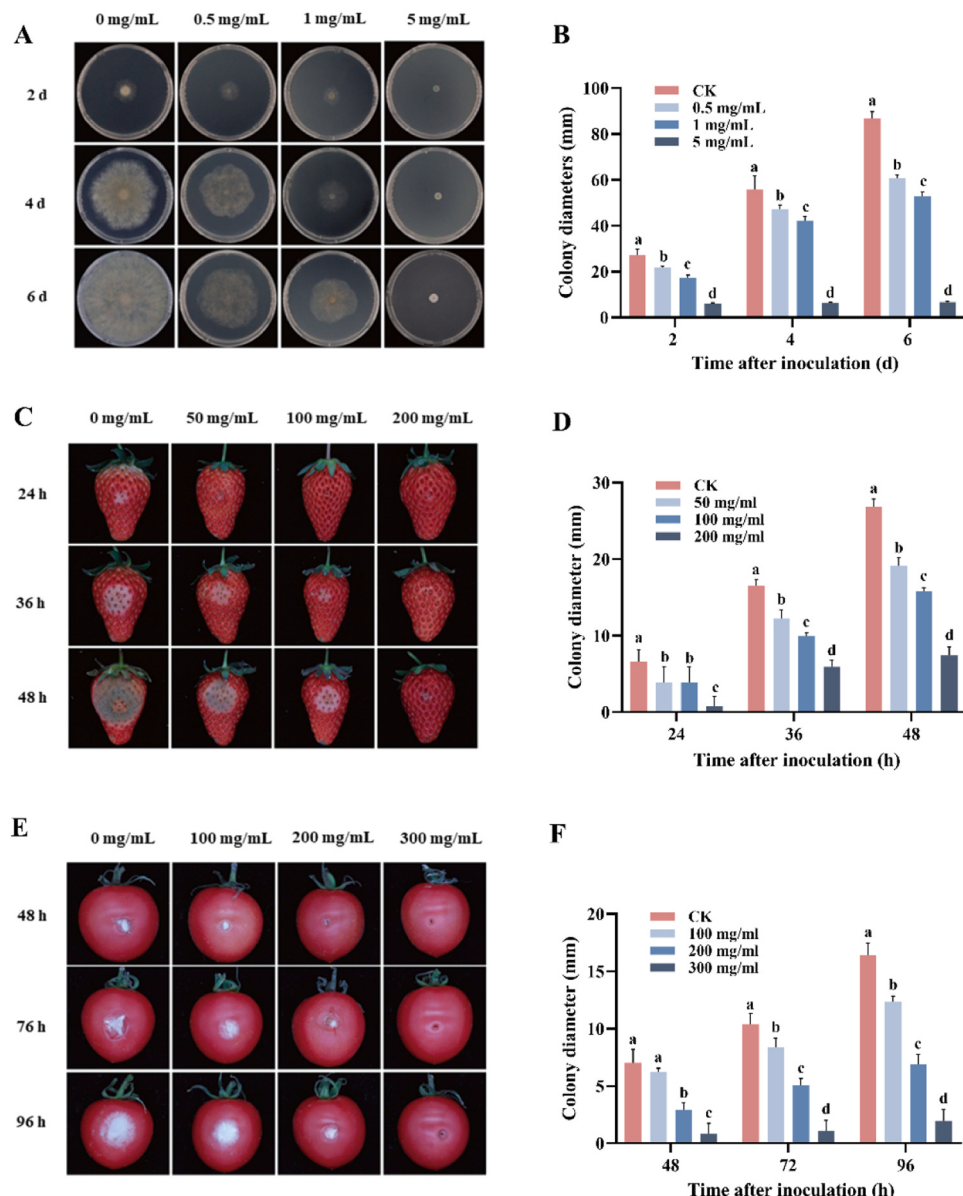


Fig. 6. Antifungal activity of PAE/HP/CD-IC *in vitro* and *in vivo*. (A and B) The morphology and colony diameter of *B. cinerea* on PDA plate after PAE/HP/CD-IC treatment. (C and D) The morphology and colony diameter of *B. cinerea* on strawberry fruit after PAE/HP/CD-IC treatment. (E and F) The morphology and colony diameter of *B. cinerea* on tomato fruit after PAE/HP/CD-IC treatment. Data were represented as mean \pm standard deviation, with six replicates for PDA plates and three replicates (each replicate containing 24 fruit) for fruit samples. Different lowercase letters in the column of the same component represented a significant difference between different groups at $p < 0.05$ level by Tukey testing.

Thus, these results indicated that the stability and antifungal activity of PAE were significantly improved after being encapsulated by HP/CD.

3.3.7. Antifungal activity of PAE/HP/CD-IC *in vitro* and *in vivo*

The *in vitro* and *in vivo* antifungal efficacy of PAE/HP/CD-IC on the growth of *B. cinerea* was shown in Fig. 6. The colony diameter of *B. cinerea* extended quickly in the control group, whereas the presence of PAE/HP/CD-IC inhibited the mycelium growth on the PDA medium. The inhibition effect was positively correlated with the concentration of the inclusion complex, and the optimal inhibition effect was observed in 5 mg/mL of PAE/HP/CD-IC. After 6 d of inoculation, the colony diameter of *B. cinerea* was only 6.73 mm at 5 mg/mL of PAE/HP/CD-IC treatment, compared to 86.88 mm in the control group. In addition, compared with the *in vitro* experiments, it was also found that a higher concentration of PAE/HP/CD-IC was needed to control grey mold disease in strawberry and tomato fruit. As shown in Fig. 6C and D, the

lesion diameter of the control group was 26.84 mm at 48 h of inoculation, and the grey mold nearly covered the whole strawberry fruit, while the lesion diameter of 200 mg/mL of PAE/HP/CD-IC treatment was only 7.44 mm. A higher concentration of PAE/HP/CD-IC (300 mg/mL) was needed to achieve the same inhibitory effects on tomato fruit, in which the lesion diameter could be reduced to 20.01% of the control group, without producing any toxic effect (Fig. 6E and F). As reported by Gao et al. (2022a), the antibacterial properties of PA were still retained after forming the complex of PA/HP γ CD-IC-NF. Furthermore, Li et al. (2022) also demonstrated that LCEO/HP β CD-IC showed certain antifungal activities against *G. citri-aurantii* and *P. italicum*, also effective for maintaining the fruit quality of 'Shatangju' mandarin. Sun et al. (2021) demonstrated that 5 mg/mL of thymol/HP β CD-IC had stronger inhibitory effects on *B. cinerea* on the PDA plate, while a higher concentration of 30 mg/mL were needed for controlling of *B. cinerea* infection on tomatoes. We also found that the effective antifungal concentration of

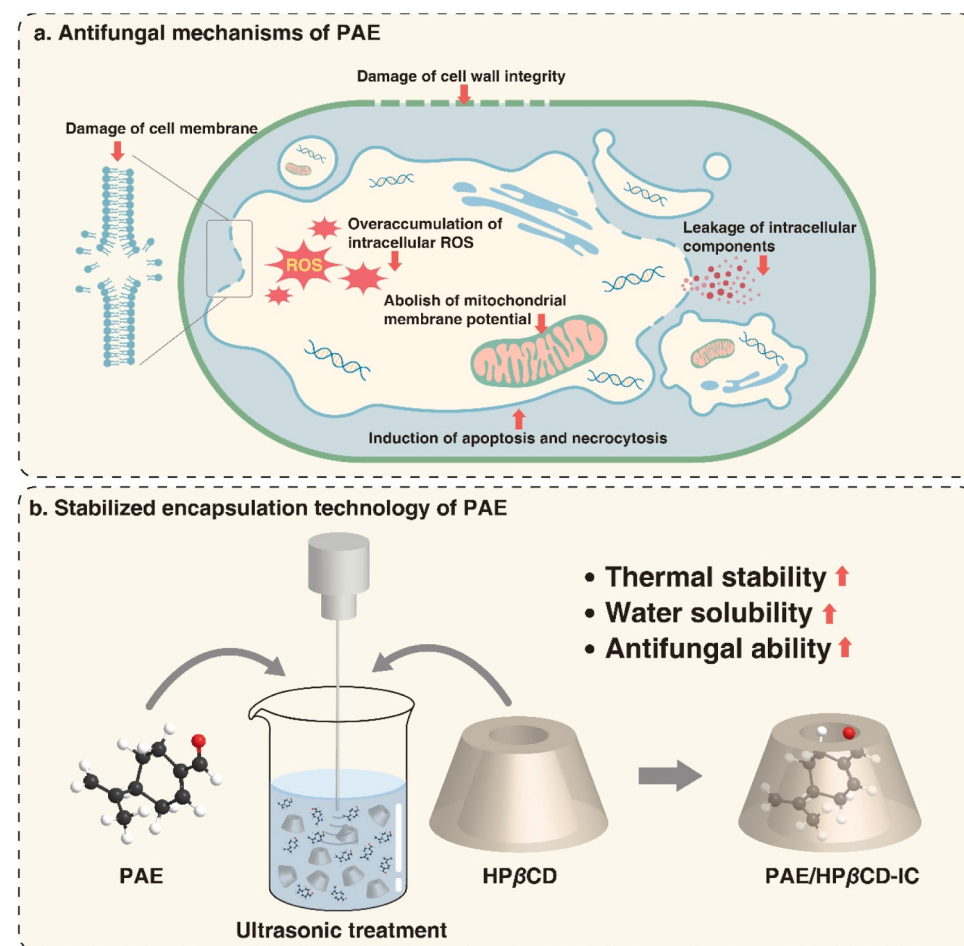


Fig. 7. A model diagram for the antifungal mechanisms (a) and stabilized encapsulation technology (b) of PAE.

PAE/HP β CD-IC applied on the fruit was significantly higher than on the plate, and the underlying mechanism needs to be further explored in the future. The current results demonstrated that the inclusion complex of PAE/HP β CD retained the antifungal activity and had promising utilization in fruit preservation.

4. Conclusion

PAE conferred promising antifungal capacity to common postharvest fungal pathogens, with the minimum inhibitory concentration of 1 μ L/mL. The antifungal mechanism of PAE was attributed to the stimulation of ROS levels, destruction of mitochondrial function, and induction of spore necrocytosis and apoptosis (Fig. 7). Furthermore, transcriptomic analysis showed that the gene expression pattern of *B. cinerea* significantly changed after PAE treatment, and the DEGs were mainly involved in the MAPK signaling pathway and cell wall integrity pathway. In order to stabilize PAE for fruit preservation, the inclusion complex of PAE/HP β CD was successfully synthesized using the ultrasonic-assisted method, as proved by UV-vis spectroscopy, FT-IR, TGA, DSC, SEM and 1 H NMR. The prepared PAE/HP β CD-IC possesses the advantages of water solubility, strong thermal stability and promising antifungal activity, which might be a promising strategy to improve the food application of PAE. Our work provided the theoretical basis for the utilization of PAE and developed a stabilized PAE/HP β CD inclusion complex for food active packaging, fruit preservation and other fields.

CRediT authorship contribution statement

Chen Kang: Investigation, Writing - original draft. He Zhang: Data

curation, Formal analysis. Cui Sun: Investigation, Methodology. Jinping Cao: Conceptualization, Writing - review & editing. Han Yang: Resources. Jiebiao Chen: Visualization, Formal analysis. Yue Wang: Conceptualization, Validation. Chongde Sun: Supervision, Project administration, Funding acquisition.

Declaration of Competing Interest

The authors declare that they have no conflict of interest.

Data Availability

Data will be made available on request.

Acknowledgement

This research was funded by the National Natural Science (32072132; 32102021; 32101932), the 111 Project (B17039) and the Key Research and Development Program of Zhejiang Province (2021C02018). We thank Nianhang Rong, Jingyao Chen and Qiong Huang from the core facility platform of Zhejiang University for their technical support.

Appendix A. Supporting information

Supplementary data associated with this article can be found in the online version at doi:10.1016/j.postharvbio.2023.112613.

References

- Abbey, J.A., Percival, D., Abbey, L., Asiedu, S.K., Prithiviraj, B., Schilder, A., 2019. Biofungicides as alternative to synthetic fungicide control of grey mould (*Botrytis Cinerea*) - prospects and challenges. *Biocontrol Sci. Technol.* 29 (3), 207–228. <https://doi.org/10.1080/09583157.2018.1548574>.
- Astray, G., Gonzalez-Barreiro, C., Mejuto, J.C., Rial-Otero, R., Simal-Gandara, J., 2009. A review on the use of cyclodextrins in foods. *Food Hydrocoll.* 23, 1631–1640. <https://doi.org/10.1016/j.foodhyd.2009.01.001>.
- Bartual, S.G., Wei, W.F., Zhou, Y., Pravataa, V.M., Fang, W.X., Yan, K.Z., Ferenbach, A.T., Lockhart, D.E.A., van Aaltena, D.M.F., 2021. The citron homology domain as a scaffold for Rho1 signaling. *Proc. Natl. Acad. Sci. USA* 118 (39), e2110298118. <https://doi.org/10.1073/pnas.2110298118>.
- Cui, H., Siva, S., Lin, L., 2019. Ultrasound processed cuminaldehyde/2-hydroxypropyl- β -cyclodextrin inclusion complex: preparation, characterization and antibacterial activity. *Ultraso. Sonochem.* 56, 84–93. <https://doi.org/10.1016/j.ulsonch.2019.04.001>.
- Gao, S., Li, X.M., Yang, G., Feng, W.W., Zong, L., Zhao, L.X., Ye, F., Fu, Y., 2022a. Antibacterial perillaldehyde/hydroxypropyl- β -cyclodextrin inclusion complex electrospun polymer-free nanofiber: improved water solubility, thermostability, and antioxidant activity. *Ind. Crops Prod.* 176, 114300 <https://doi.org/10.1016/j.indcrop.2021.114300>.
- Gao, S., Feng, W.W., Sun, H., Zong, L., Li, X.M., Zhao, L.X., Ye, F., Fu, Y., 2022b. Fabrication and characterization of antifungal hydroxypropyl- β -cyclodextrin/pyrimethanil inclusion compound nanofibers based on electrospinning. *J. Agr. Food Chem.* 70, 7911–7920. <https://doi.org/10.1021/acs.jafc.2c01866>.
- Gao, S., Zong, L., Zhang, Y.H., Zhang, Y., Guo, X.Y., Guo, G.H., Zhao, L.X., Ye, F., Fu, Y., 2023. Antifungal pentachloronitrobenzene/hydroxypropyl-beta-cyclodextrin inclusion complex nanofibers by electrospun with no polymer fabrication and characterization. *J. Clean. Prod.* 413, 137499 <https://doi.org/10.1016/j.jclepro.2023.137499>.
- He, C., Zhang, Z.Q., Li, B.Q., Xu, Y., Tian, S.P., 2019. Effect of natamycin on *Botrytis cinerea* and *Penicillium expansum*—postharvest pathogens of grape berries and jujube fruit. *Postharvest Biol. Technol.* 151, 134–141. <https://doi.org/10.1016/j.postharvbio.2019.02.009>.
- Higuchi, T., Connors, K.A., 1965. Phase-solubility techniques. *Adv. Anal. Chem. Instrum.* 4, 117–212.
- Hwang, J.H., Hwang, I., Liu, Q., Woo, E., Lee, D.G., 2012. (+)-Medioresinol leads to intracellular ROS accumulation and mitochondria-mediated apoptotic cell death in *Candida albicans*. *Biochimie* 94 (8), 1784–1793.
- Islahudin, F., Khozoei, C., Bates, S., Ting, K.N., Pleass, R.J., Avery, S.V., 2013. Cell wall perturbation sensitizes fungi to the antimalarial drug chloroquine. *Antimicrob. Agents Chemother.* 57, 3889–3896. <https://doi.org/10.1128/AAC.00478-13>.
- Jiang, S., Zhao, T.T., Wei, Y.Y., Cao, Z.D., Xu, Y.Y., Wei, J.Y., Xu, F., Wang, H.F., Shao, X.F., 2021. Preparation and characterization of tea tree oil/hydroxypropyl- β -cyclodextrin inclusion complex and its application to control brown rot in peach fruit. *Food Hydrocoll.* 121, 107037 <https://doi.org/10.1016/j.foodhyd.2021.107037>.
- Kang, C., Jiang, A.Z., Yang, H., Zheng, G.X., Wang, Y., Cao, J.P., Sun, C.D., 2022. Integrated physicochemical, hormonal and transcriptomic analysis revealed the underlying mechanisms for granulation in Huyou (*Citrus changshensis*) fruit. *Front. Plant Sci.* 13, 923443 <https://doi.org/10.3389/fpls.2022.923443>.
- Li, X., Li, G., Shan, Y., Zhu, X., 2022. Preparation, characterization, and antifungal property of the inclusion complex of Litsea cubeba essential oil/hydroxypropyl- β -cyclodextrin and its application in preservation of Shatang mandarin. *J. Food Sci.* 87, 4714–4724. <https://doi.org/10.1111/1750-3841.16313>.
- Liu, X.Y., Ji, D.C., Cui, X.M., Zhang, Z.Q., Li, B.Q., Xu, Y., Chen, T., Tian, S.P., 2020. p-Coumaric acid induces antioxidant capacity and defense responses of sweet cherry fruit to fungal pathogens. *Postharvest Biol. Technol.* 169, 111297 <https://doi.org/10.1016/j.postharvbio.2020.111297>.
- Liu, Y.Y., Zhao, C., Huang, M.L., Sun, C., Cao, J.P., Wang, J.Y., Huang, L.X., 2022. Effect of cold atmospheric plasma on the gray mold rot of postharvest mulberry fruit. *Food Control* 137, 108906. <https://doi.org/10.1016/j.foodcont.2022.108906>.
- Ma, H.L., Yang, L.B., Tian, Z.Q., Zhu, L.J., Peng, J., Fu, P., Xiu, J.F., Guo, G., 2023. Antimicrobial peptide AMP-17 exerts anti-*Candida albicans* effects through ROS-mediated apoptosis and necrosis. *Int. Microbiol.* 26, 81–90. <https://doi.org/10.1007/s10123-022-00274-5>.
- Negi, J.S., Singh, S., 2013. Spectroscopic investigation on the inclusion complex formation between amisulpride and γ -cyclodextrin. *Carbohydr. Polym.* 92 (2), 1835–1843. <https://doi.org/10.1016/j.carbpol.2012.11.082>.
- Pan, C., Li, Y.X., Yang, K.L., Famous, E., Ma, Y., He, X.N., Geng, Q.R., Liu, M., Tian, J., 2020. The molecular mechanism of perillaldehyde inducing cell death in *Aspergillus flavus* by inhibiting energy metabolism revealed by transcriptome sequencing. *Int. J. Mol. Sci.* 21, 1518. <https://doi.org/10.3390/ijms21041518>.
- Pu, H.Y., Sun, Q.M., Tang, P.X., Zhao, L.D., Li, Q., Liu, Y.Y., Li, H., 2018. Characterization and antioxidant activity of the complexes of tertiary butylhydroquinone with β -cyclodextrin and its derivatives. *Food Chem.* 260, 183–192. <https://doi.org/10.1016/j.foodchem.2018.04.008>.
- Romanazzia, G., Sanzani, S.M., Bi, Y., Tian, S.P., Martínez, P.G., Alkan, N., 2016. Induced resistance to control postharvest decay of fruit and vegetables. *Postharvest Biol. Technol.* 122, 82–94. <https://doi.org/10.1016/j.postharvbio.2016.08.003>.
- Sato, K., Krist, S., Buchbauer, G., 2006. Antimicrobial effect of trans-cinnamaldehyde, (-)-perillaldehyde, (-)-citronellal, citral, eugenol and carvacrol on airborne microbes using an airwasher. *Biol. Pharm. Bull.* 29, 2292–2294.
- Shu, C., Zhao, H., Jiao, W., Liu, B., Cao, J., Jiang, W., 2019. Antifungal efficacy of ursolic acid in control of *Alternaria alternata* causing black spot rot on apple fruit and possible mechanisms involved. *Sci. Hortic.* 256, 108636 <https://doi.org/10.1016/j.scientia.2019.108636>.
- Sun, C., Cao, J.P., Wang, Y., Chen, J.B., Huang, L.X., Zhang, H., Wu, J., Sun, C.D., 2021. Ultrasound-mediated molecular self-assemble of thymol with 2-hydroxypropyl- β -cyclodextrin for fruit preservation. *Food Chem.* 363, 130327 <https://doi.org/10.1016/j.foodchem.2021.130327>.
- Sun, C., Cao, J.P., Wang, Y., Huang, L.X., Chen, J.B., Wu, J., Zhang, H., Chen, Y.Y., Sun, C.D., 2022. Preparation and characterization of pectin-based edible coating agent encapsulating carvacrol/HP/CD inclusion complex for inhibiting fungi. *Food Hydrocoll.* 125, 107374 <https://doi.org/10.1016/j.foodhyd.2021.107374>.
- Tang, D.L., Chen, X., Kroemer, G., 2022. Cuproptosis: a copper-triggered modality of mitochondrial cell death. *Cell Res.* 32, 417–418. <https://doi.org/10.1038/s41422-022-00653-7>.
- Tang, P., Li, S., Wang, L., Yang, H., Yan, J., Li, H., 2015. Inclusion complexes of chloroxazone with beta- and hydroxypropyl-beta-cyclodextrin: characterization, dissolution, and cytotoxicity. *Carbohydr. Polym.* 131, 297–305. <https://doi.org/10.1016/j.carbpol.2015.05.055>.
- Tian, J., Wang, Y., Zeng, H., Li, Z., Zhang, P., Tessema, A., Peng, X., 2015. Efficacy and possible mechanisms of perillaldehyde in control of *Aspergillus Niger* causing grape decay. *Int. J. Food Microbiol.* 202, 27–34. <https://doi.org/10.1016/j.ijfoodmicro.2015.02.022>.
- Tian, J., Pan, C., Zhang, M., Gan, Y.Y., Pan, S.Y., Liu, M., Li, Y.X., Zeng, X.B., 2019. Induced cell death in *Ceratostys fimbriata* by pro-apoptotic activity of a natural organic compound, perillaldehyde, through Ca^{2+} overload and accumulation of reactive oxygen species. *Plant Pathol.* 68, 344–357. <https://doi.org/10.1111/ppa.12937>.
- Wang, J., Cao, Y.P., Sun, B.G., Wang, C.T., 2011. Characterization of inclusion complex of trans-ferulic acid and hydroxypropyl- β -cyclodextrin. *Food Chem.* 124, 1069–1075. <https://doi.org/10.1016/j.foodchem.2010.07.080>.
- Yang, S.Z., Yan, D., Li, M., Li, D.M., Zhang, S.X., Fan, G., Peng, L.T., Pan, S.Y., 2022. Ergosterol depletion under bifonazole treatment induces cell membrane damage and triggers a ROS-mediated mitochondrial apoptosis in *Penicillium expansum*. *Fungal Biol.* 126, 1–10. <https://doi.org/10.1016/j.funbio.2021.09.002>.
- Yao, Y.S., Xie, Y., Hong, C., Li, G.W., Shen, H.Y., Ji, G., 2014. Development of a myricetin/hydroxypropyl- β -cyclodextrin inclusion complex: preparation, characterization, and evaluation. *Carbohydr. Polym.* 110 (22), 329–337. <https://doi.org/10.1016/j.carbpol.2014.04.006>.
- Yildiz, Z.I., Kilic, M.E., Durgun, E., Uyar, T., 2019. Molecular encapsulation of cinnamaldehyde within cyclodextrin inclusion complex electrospun nanofibers: fast-dissolution, enhanced water solubility, high temperature stability, and antibacterial activity of cinnamaldehyde. *J. Agr. Food Chem.* 67, 11066–11076. <https://doi.org/10.1021/acs.jafc.9b02789>.
- Yuan, C., Jin, Z., Xu, X., Zhuang, H., Shen, W., 2008. Preparation and stability of the inclusion complex of astaxanthin with hydroxypropyl- β -cyclodextrin. *Food Chem.* 109, 264–268. <https://doi.org/10.1016/j.foodchem.2007.07.051>.
- Zhang, M., Liu, M., Pan, S.Y., Pan, C., Li, Y.X., Tian, J., 2018. Perillaldehyde controls postharvest black rot caused by *Ceratostys fimbriata* in sweet potatoes. *Front. Microbiol.* 9, 1102. <https://doi.org/10.3389/fmicb.2018.01102>.
- Zhou, Q.N., Wei, X.H., Dou, W., Chou, G.X., Wang, Z.T., 2013. Preparation and characterization of inclusion complexes formed between baicalein and cyclodextrins. *Carbohydr. Polym.* 90 (2), 733–739. <https://doi.org/10.1016/j.carbpol.2013.02.038>.